Gaussian core model in two dimensions. II. Solid and fluid phase topological distribution functions

Thomas A. Weber and Frank H. Stillinger

Bell Laboratories, Murray Hill, New Jersey 07974
(Received 20 November 1980; accepted 12 December 1980)

Local structure in the two-dimensional Gaussian core model at $\rho^* = 3^{-1/2}$ has been anayzed through the topology of nearest-neighbor polygons. Disorder is revealed by the presence of nonhexagonal polygons (disclinations). Near the melting point most disclination polygons have either five or seven sides and these are present in nearly equal concentrations. The concentrations increase by an order of magnitude upon melting the solid. Within the melting range phase coexistence is revealed by inhomogeneous distribution of disclinations. Pair correlation functions have been calculated for particles classified by polygon character; they show asymmetry with respect to disclination type. The first-order melting process can be described as condensation of a dilute gas of small disclination aggregates (solid phase) into a dense medium of disclinations (fluid phase).

I. INTRODUCTION

The first paper of this series[1] initiated an examination of melting in the two-dimensional Gaussian core model at reduced density $\rho^* = 3^{-1/2}$. Thermodynamic functions and particle pair correlation functions generated by molecular dynamics simulation displayed behavior indicative of a simple first-order transition. In this paper we extend the study of that transition by observing the distribution of Wigner–Seitz (or Voronoi) cells.[2] The results confirm and strengthen the prior conclusion about transition order, and in addition they offer a clear and convenient means to describe the melting process and the disordered fluid it produces.

The nearest-neighbor Wigner–Seitz polygon for particle j is the open set of points in the plane closer to j than to any other particle. It can be constructed by erecting perpendicular bisectors to all lines connecting j to other particles, and then selecting that subset of bisectors which encloses a minimum area. The nearest-neighbor polygons are convex, contain only single particles, and partition the plane without overlaps. They also generate a nearest-neighbor topology, for pairs of particles whose polygons share a common side are defined to be "nearest neighbors."

The lowest energy structure at all densities for Gaussian core particles [pair potential $\exp(-r_{ij}^2)$] is the regular triangular lattice. The Wigner–Seitz cells then are identical regular hexagons as Fig. 1(a) illustrates. If the particles undergo small relative displacements (as created, for example, by harmonic phonon motion) the hexagons will distort somewhat but will remain hexagonal, i.e., the nearest-neighbor topology persists. Figure 1(b) shows the distortion produced by small displacement of a single particle in an otherwise perfect triangular array.

The principal advantage of the Wigner–Seitz cells is their diagnostic ability for distortions large enough to change neighbor topology. Figure 1(c) exhibits the geometric result of inserting an extra particle, an interstitial, with displacement of a neighbor to create a symmetrically dislocated pair. This process generates a localized 5–7–5–7 tetrad with pentagons sharing a side. It might be noted in passing that a similar tetrad, but with the heptagons sharing a side, can be produced by a shearing strain applied to a compact group of four particles in the undisturbed lattice.

A 5–7 dyad constitutes a dislocation whose Burgers vector[3] is related to the dyad axis. The pattern in Fig. 1(c) is a neighboring dislocation pair with canceling Burgers vectors. Figures 1(d) and 1(e) show examples with more widely separated dislocation pairs, i.e., 5–7 dyads. Thermally driven separation of dislocation pairs plays a central role in the melting theory of Halperin and Nelson[4,5] that was based on prior work of Kosterlitz and Thouless.[6]

A closed loop of 5–7 dyads signals the existence of a grain boundary. Figure 1(f) exhibits a simple example in which seven interior particles have been rotated 30° with respect to the surrounding lattice to produce a "hexatic daisy." More complex grain boundaries of sets of rotated particles have been observed in the spontaneously frozen solid, as reported in the previous paper.[1]

With these elementary examples as background we proceed in Sec. II to the construction and enumeration of Wigner–Seitz cells for the actual particle configurations that occur in the Gaussian core system. The four specific thermodynamic states selected for study were generated from the work of Ref. 1 on a system of 780 particles.

Section III examines the various pair distribution functions that can be defined for particles distinguished by the numbers of sides to their polygons. Although the fractional concentrations n_i of these particle species present an approximate symmetry about n_6, that symmetry obviously does not extend to the pair distribution functions.

We conclude this paper in Sec. IV with a discussion of the melting process as phrased in terms of the neighbor topology.

 0021-9606/81/074020-09$01.00

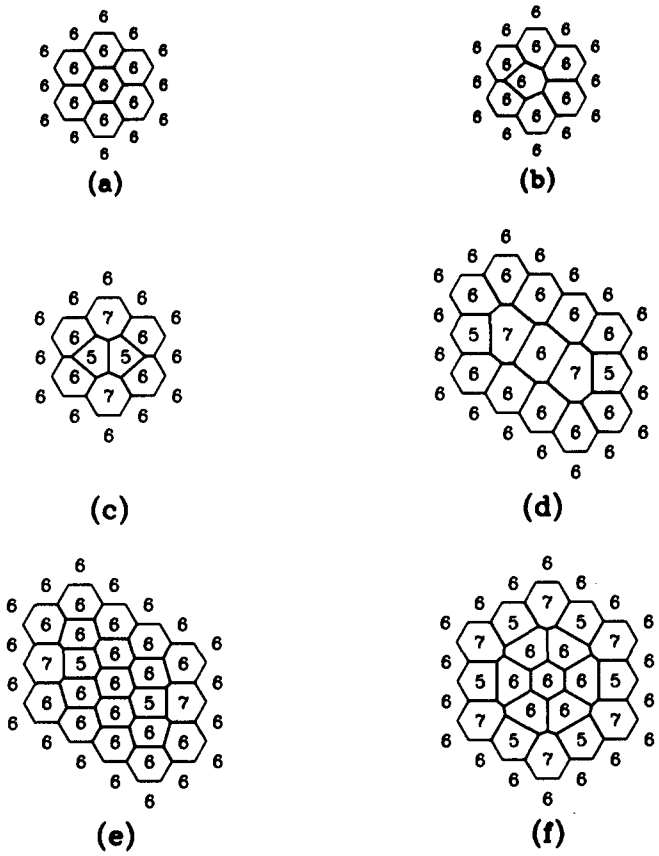

FIG. 1. Wigner–Seitz polygons for small clusters of particles. (a) Perfect triangular lattice; (b) small horizontal displacement of a single particle; (c) extra particle (interstitial) with symmetrical displacement of a pair; (d) and (e) separated dislocations (each a 5–7 dyad); (f) rotational grain boundary.

II. POLYGON CONCENTRATIONS

Table I lists the fractional concentrations (mole fractions) n_i of i-sided polygons that have been computed for four distinct thermodynamic states. The respective reduced temperatures T^*, pressures p^*, and mean interaction energies per particle $\langle\Phi\rangle/N$ are also listed. The reduced density ρ^* has the common value $3^{-1/2}$ for each. State A is a crystal aligned with the sides of the periodic unit cell; it is slightly superheated (the melting temperature T_m^* is thought to be about 6.6×10^{-3}), but it is indefinitely stable as such since no nucleation sites are present to initiate the melting process. State B lies near the midpoint of the melting range, and was identified[1] as exhibiting phase coexistence. States C and D involve the homogeneous fluid, with the former just below the thermodynamic freezing temperature $T_f^* = 7.2\times10^{-3}$.

We can supplement the data in Table I with the observation that all nonhexagonal polygons become very rare in the crystal as the temperature declines substantially below the melting range. For this reason no further crystalline states were analyzed.

A glance at Table I shows that the occurrence frequency of nonhexagonal polygons depends strongly on the state. By comparing n_5 and n_7 for states A and C, for example, one sees that melting creates a tenfold increase in the concentrations of these species. For this reason we felt obliged to use a longer molecular dynamics run for state A, the crystal, than for the other states as the last line in Table I indicates.

The average number of sides for the nearest-neighbor polygons is six, reagardless of the state[7];

$$\langle i\rangle = \sum_i i n_i = 6 \ . \tag{2.1}$$

This result can be deduced from Euler's theorem.[8] It also can be established by the following elementary geometric argument. Note first that (aside from zero-probability coincidences) polygon sides always come together in triplets, i.e., three polygons meet at each vertex point. Therefore the average number of such vertices per particle in the plane is simply

$$v = \tfrac{1}{3}\langle i\rangle \ . \tag{2.2}$$

Of course, the sum of vertex angles at these points is 2π, so that

$$2\pi v = 2\pi\langle i\rangle/3 \tag{2.3}$$

is the average value of the interior angle sum for the polygons. On the other hand, every i-sided polygon has $\pi(i-2)$ for this sum, so on average

$$2\pi\langle i\rangle/3 = \pi(\langle i\rangle - 2) \ , \quad \langle i\rangle = 6 \ . \tag{2.4}$$

The results in Table I show that in the temperature range examined, virtually all of the nonhexagonal polygons had either five or seven sides. Although four and eight-sided cases occur, they are quite rare. No triangles or polygons with more that eight sides were ever observed. The inviolate condition (2.4) hence has the practical result that n_5 and n_7 are nearly equal. In other words, the polygon size distribution is nearly symmetrical about $i=6$.

At very high temperature we expect some skewing of this symmetrical distribution as polygons with $i \geq 9$

TABLE I. Selected properties of four thermodynamic states for the Gaussian core model in two dimensions at reduced density $3^{-1/2}$.

	A Crystal	B Coexistence	C Fluid	D Fluid
$10^3\ T^*$	7.017 3	6.954 6	7.016 7	8.695 0
p^*	0.498 044 9	0.496 447 4	0.495 534 2	0.495 240 6
$\langle\Phi\rangle/N$	0.422 007 6	0.423 247 8	0.424 015 8	0.426 087 5
n_4	0.000 01	0.000 27	0.000 46	0.000 89
n_5	0.012 29	0.077 39	0.120 67	0.147 82
n_6	0.975 40	0.844 56	0.757 61	0.702 84
n_7	0.012 30	0.077 63	0.120 92	0.147 30
n_8	0.000 00	0.000 15	0.000 34	0.001 15
number of steps[a]	16000	8000	4000	4000

[a]The incremental time step Δt^* for integration of the dynamical equations was 0.05 throughout this study.

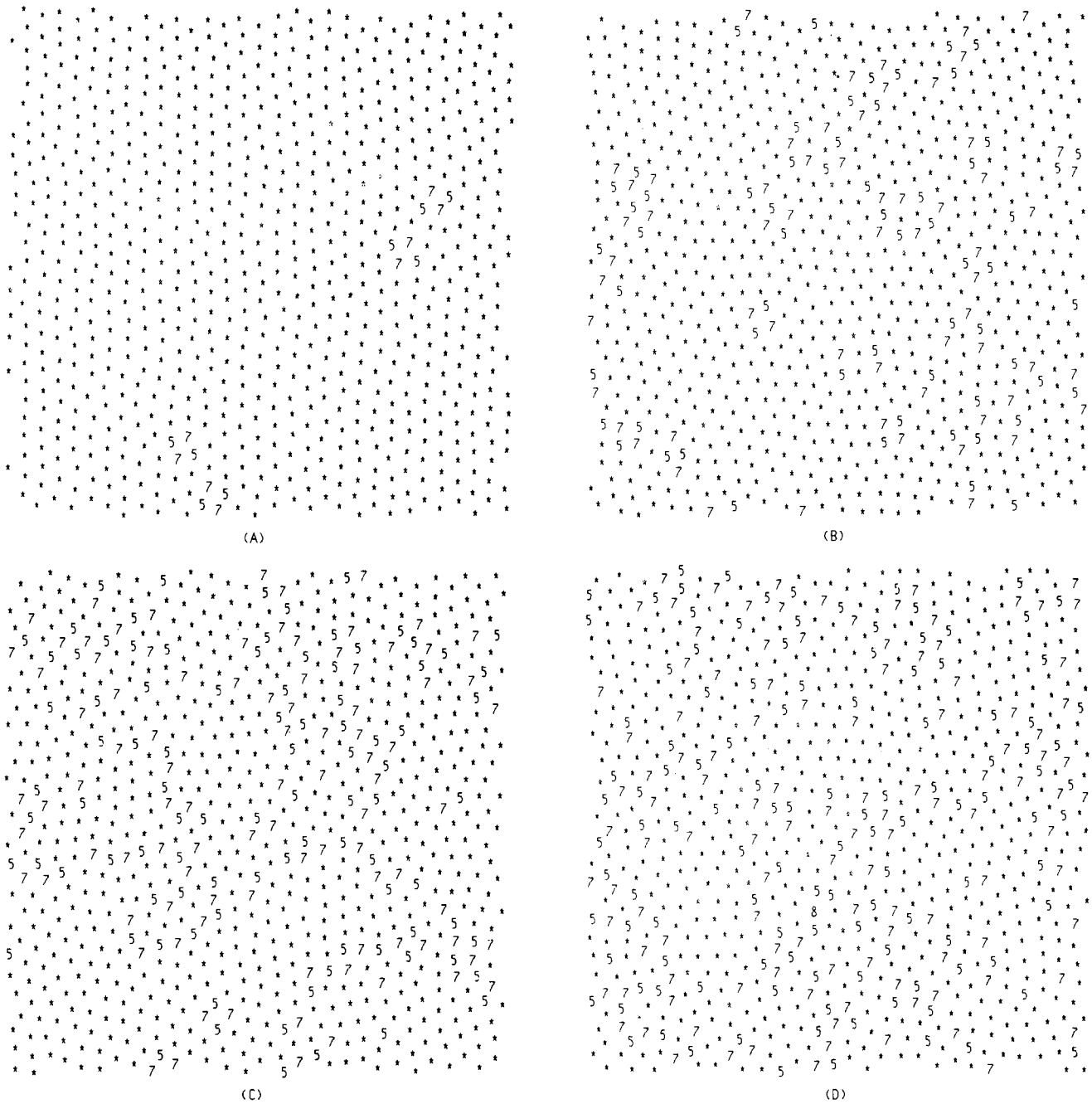

FIG. 2. Snapshots of Wigner-Seitz polygons for the 780-particle simulations at density $\rho^* = 3^{-1/2}$ for the four thermodynamic states: (A) superheated crystal; (B) transition region; (C) and (D) fluid. The hexagons are identified as asterisks.

begin to make an appearance.

Figures 2(A)–2(D) show configurations of the 780 particle system at the end of each of the four runs *A–D*. Particles within hexagons are rendered as asterisks for simplicity while integers ≠ 6 locate the other species. We have monitored each of these four states in this pictorial way during its chronological development (as well as many other states in our overall study[1]) and have found that: (a) the patterns of polygons are very variable over each run indicating good sampling statistics, and that (b) the overall character of each state is reasonably well represented by the specific configurations shown in Figs. 2(A)–2(D).

In the crystalline state Fig. 2(A), only a small number of disclination polygons appear, and these are all clustered into tetrads. The tetrads have arisen essentially from large-amplitude local shearing motions that undoubtedly are connected with anharmonic behavior of this high-temperature crystal.

Figure 2(B) shows the system in the middle of its fixed-density melting range. Disclination polygons are much commoner, and not at all restricted to tetrads of the type shown in Fig. 2(A). 5–7 dyads (dislocations) show a tendency to unpair, and to form rudimentary grain boundaries. The distribution of disclination polygons in the large is nonuniform, with substantial areas con-

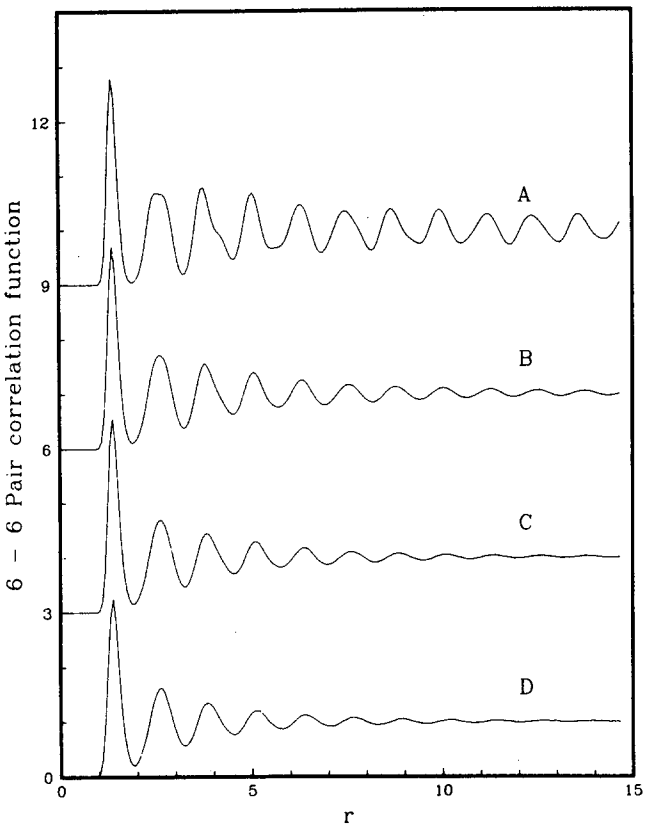

FIG. 3. Hexagon–hexagon pair correlation functions g_{66} for the four thermodynamic states listed in Table I.

taining none (except for anharmonic-crystal-like tetrads), while other regions contain high concentrations in complex arrangements. We associate this nonuniformity with phase coexistence, though admittedly it is difficult to draw boundaries between coexisting phases unambiguously.

The melting process presumably is completed in Fig. 2(C), wherein elements of grain boundaries appear to run throughout the system. Note, however, that in the topological sense there still remain small domains of crystalline order. The lines of particles which low-angle viewing shows to run frequently across Fig. 2(B) are substantially broken up in Fig. 2(C).

Further rise in temperature, Fig. 2(D), reduces the mean range of topological order. In a high-density medium of disclinations such as this it is obviously unclear how to classify local polygon arrangements since dyads, tetrads, etc. do not occur in isolation.

A lone octagon can be found in Fig. 2(D) in the lower middle region, but no quadrilateral is present in this specific configuration. Note that the octagon is flanked by two opposing pentagons with which it shares sides. This is a rather frequent arrangement when octagons are present. We have also found that a quadrilateral, when present, is likely to be flanked by a pair of opposing heptagons with which it shares sides.

III. TOPOLOGICAL PAIR DISTRIBUTION FUNCTIONS

Once the particles in the system have been classified by polygon type it can be helpful in attempting to understand patterns present to have pair correlation functions for the various species. Let N_i at any instant be the number of particles present possessing i-sided polygons. The pair correlation function $g_{ij}^{(2)}$ for species i and j is defined so that the quantity

$$\langle N_i(N_j - \delta_{ij})\rangle\, g_{ij}^{(2)}(\mathbf{r}_{12})\, d\mathbf{r}_1\, d\mathbf{r}_2 / A^2 \qquad (3.1)$$

equals the probability for differential space elements $d\mathbf{r}_1$ and $d\mathbf{r}_2$ simultaneously to contain distinct particles of species i and j, respectively. In this expression, δ_{ij} is the Kronecker delta function and A is the system area. In a sufficiently large system every $g_{ij}^{(2)}$ can be expected to approach unity as r_{12} becomes large, regardless of thermodynamic state. Deviations of the $g_{ij}^{(2)}$ from unity at small r_{12} reveal local order.

We have evaluated angle-averaged pair correlation functions $g_{ij}(r)$ for the four states A, B, C, and D. Since the polygon side index i varies between four and eight in the present study there are in principle 15 separate functions for each state. However, since so few quadrilaterals and octagons were observed even in the highest temperature case Fig. 2(D), g_{44}, g_{48}, and g_{88} have low statistical significance and will not be displayed here.

Figure 3 shows g_{66} for the four thermodynamic states. The lattice structure and its persistence with increasing distance in the crystal are evident from curve (A). [Note that the maximum distance $r = 14.7$ in this and subsequent figures is about 0.45 of the unit cell size.] Since most particles are hexagonal in the crystal, g_{66} is very similar for that state to the species-indepen-

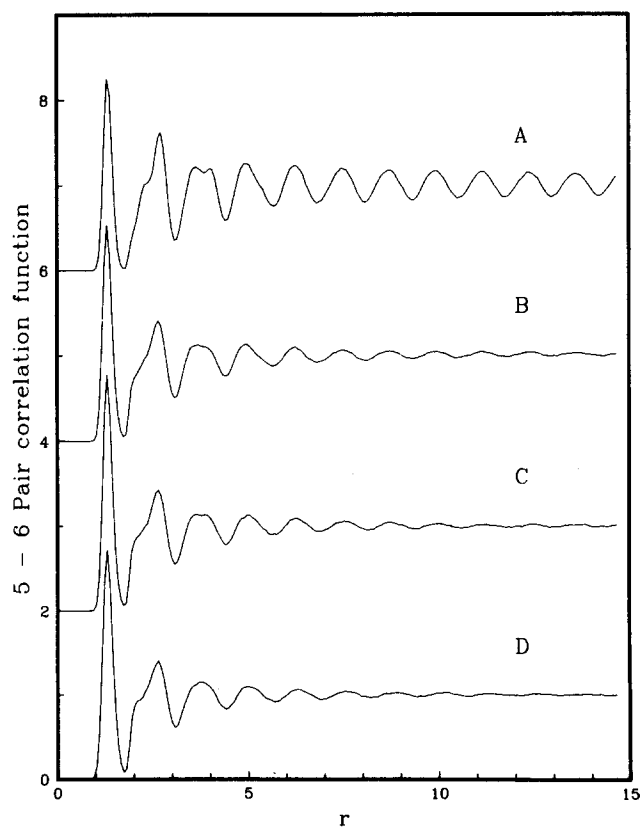

FIG. 4. Pentagon–hexagon pair correlation functions g_{56} for the four thermodynamic states listed in Table I.

dent pair correlation function g reported in the previous paper. In all four curves of Fig. 3 the first maximum is located very close to $r=2^{1/2}$, the nearest-neighbor separation in the $T^*=0$ perfect lattice.

In contrast to the persistent order in the crystal, the fluid-state curves, Figs. 3(C) and 3(D), damp to unity within the available spatial range, clearly indicating a qualitatively different type of particle packing. Numerically, we find that these fluid-phase functions have decay envelopes that appear to be exponential.

The melting-range curve Fig. 3(B) has somewhat persistent oscillations, though considerably diminished in comparison with the crystal. This is the behavior to be expected with fluid–crystal coexistence wherein large patches of the latter experience fluctuating strains due to the presence of grain boundaries and fluid-filled cracks.

Figure 4 shows the g_{56} functions, and Fig. 5 shows the g_{67} functions. The first peak of g_{56} falls at slightly smaller r than that of g_{66}, while the first peak of g_{67} falls at slightly larger r than that of g_{66}. This makes sense for repelling particles, since a "collar" of seven particles around a central one will be crowded and will be forced outward on the average. A "collar" of only six can settle inward slightly, and one of five even more. Thus on the shortest distance scale for the problem, pentagonal particles will be in high-density spots, while heptagonal particles will be in low-density spots.

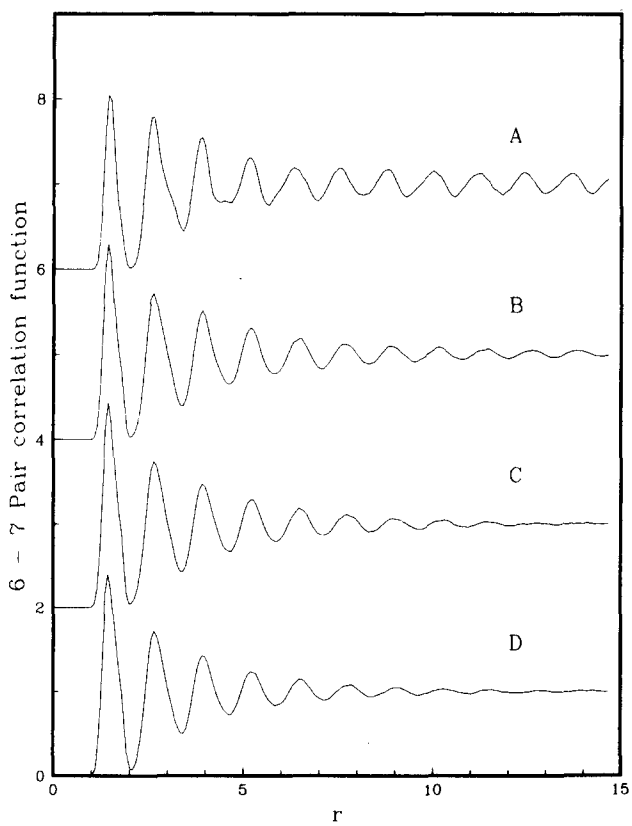

FIG. 5. Hexagon–heptagon pair correlation functions g_{67} for the four thermodynamic states listed in Table I.

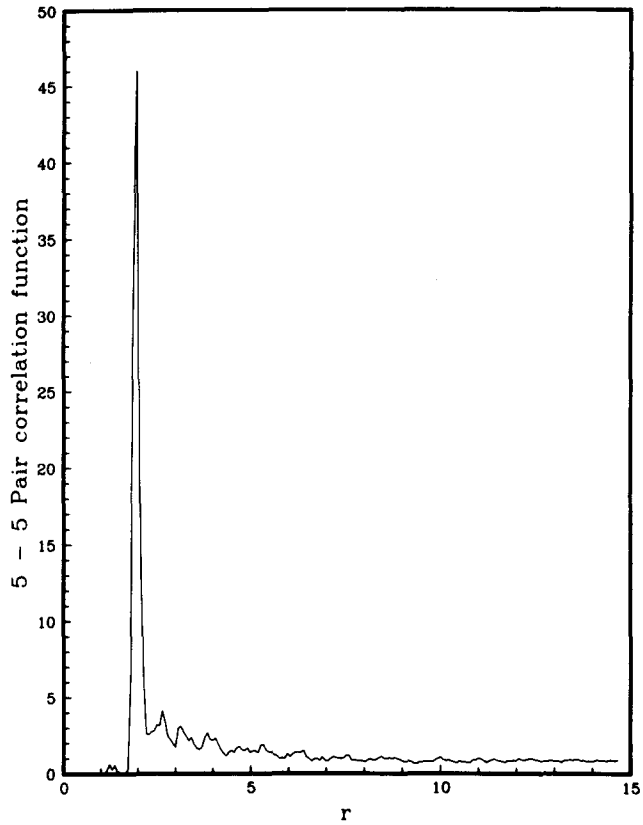

FIG. 6. Pentagon–pentagon pair correlation function g_{55} for the crystalline state A.

The fundamental asymmetry between pentagonal and heptagonal particles shows up clearly in Figs. 4 and 5. Specifically, the second and third peaks have very different shapes for g_{56} in comparison with g_{67} in all states of the system. In addition, the successive peaks of g_{67} in the fluid have distinctly greater amplitudes than those of g_{56}, and are displaced outward by roughly a constant "phase shift." These latter distinctions are not clearly evident for the crystalline state. In any case, the concentration symmetry about $i=6$ pointed out in the preceding Sec. II is obviously violated at the geometric level of pair correlation.

Figure 6 shows g_{55} for the crystal while Fig. 7 shows results for the same function in the other three states. The very large peak for the crystal ($g_{55}\approx 46$) arises from pairs of five's within the same tetrad, but *not* sharing a common side; these are formed by the local shearing motion. The very small peak at even shorter distance apparently signifies very infrequent occurrence of interstitial structures in which the two pentagons in a tetrad *do* share a side and thus are closer. Beyond the very large peak in Fig. 6 we see that g_{55} has a substantial region where it remains well above the asymptotic value unity. This indicates a marked clustering tendency for five's in the solid. Figure 7 demonstrates that melting dramatically reduces the magnitude of the large peak [to approximately three in Fig. 7(C)] while also reducing the clustering range.

Figures 8 and 9 show our results for g_{77}. The large first peak in the solid (Fig. 8) has the same source as

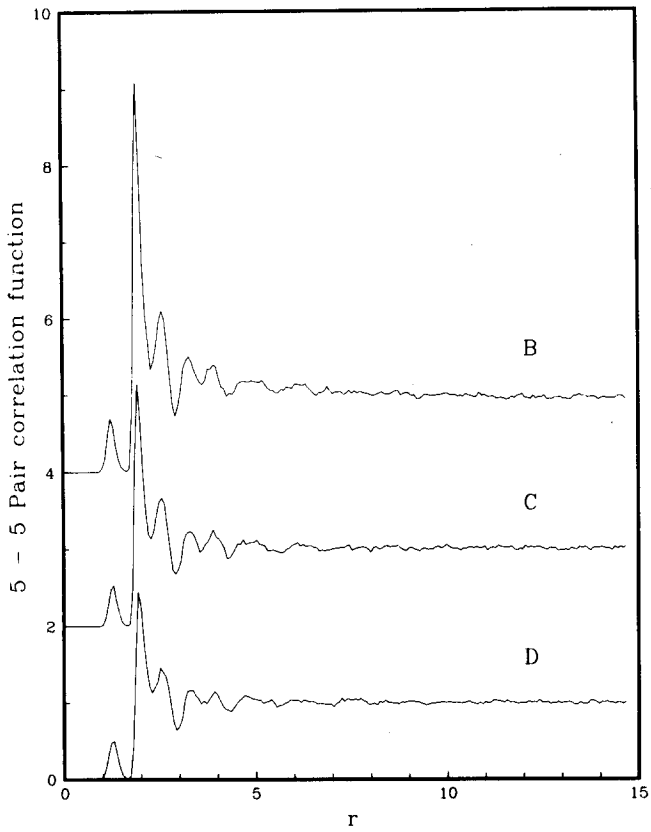

FIG. 7. Pair correlation functions g_{55} for states B, C, and D.

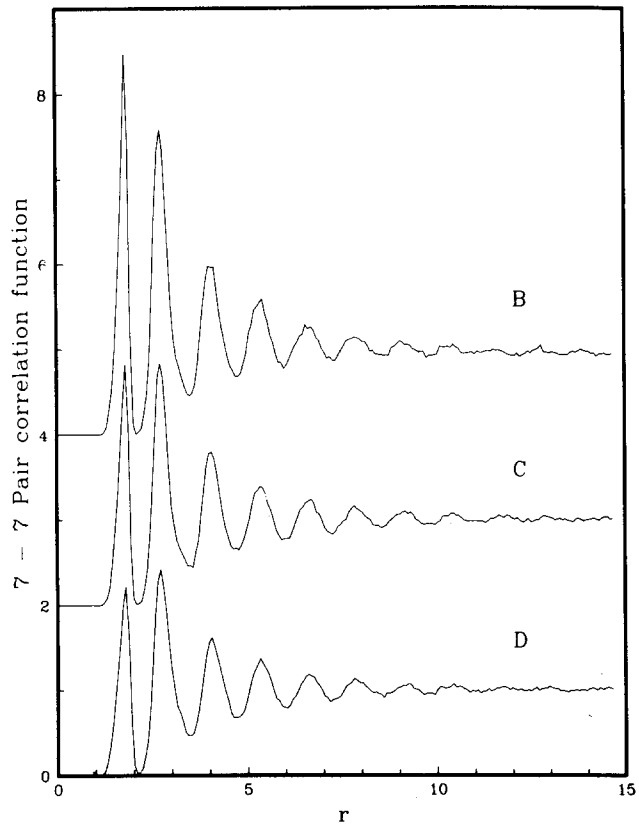

FIG. 9. Pair correlation functions g_{77} for states B, C, and D.

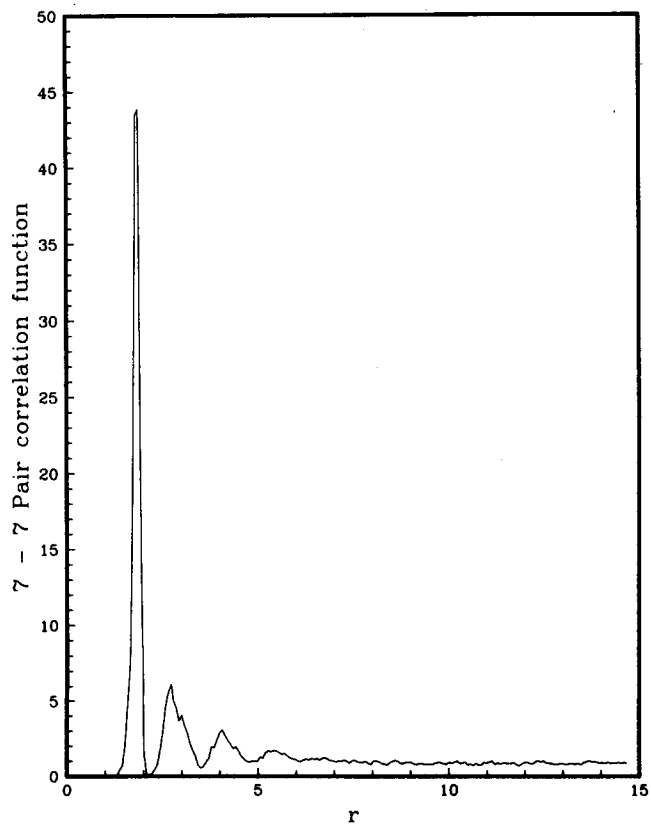

FIG. 8. Heptagon–heptagon pair correlation function g_{77} for the crystalline state A.

that in g_{55}, namely the tetrads produced by local shear. Notice, however, that this g_{77} peak occurs at somewhat smaller distance than does the corresponding g_{55} peak, symptomatic of the fact that for these (noninterstitial) tetrads it is the heptagons which share a side rather than the pentagons.

By comparing respective curves from Figs. 6 and 7 on the one hand with those from Figs. 8 and 9 on the other hand, one again confirms the lack of symmetry about $i=6$. This is particularly noticeable as regards the relatively long-ranged oscillations that appear in the fluid-phase g_{77}'s, Figs. 9(C)–(D), in contrast to the more featureless g_{55}'s, Figs. 7(C)–(D). Our examination of many fluid-phase pictures suggests a reason for this latter difference, namely that heptagons tend to be aligned in rows with roughly even spacing with the pentagons loosely flanking such collineations.

In view of what has already been stated it seems inevitable that 5–7 pairs would have to be strongly correlated at small distance. Indeed this is confirmed in the solid-phase g_{57}, Fig. 10, and in the coexistence and fluid phase g_{57}'s, Fig. 11. The large first peak in each of these four curves again reflects the existence of shear tetrads.

Pair distribution functions involving particles in quadrilaterals are shown in Figs. 12–14. Because of unfavorable statistics we have not shown curves for the crystalline state A. It is obvious from g_{45} in Fig. 12 that quadrilaterals and pentagons will not reside next

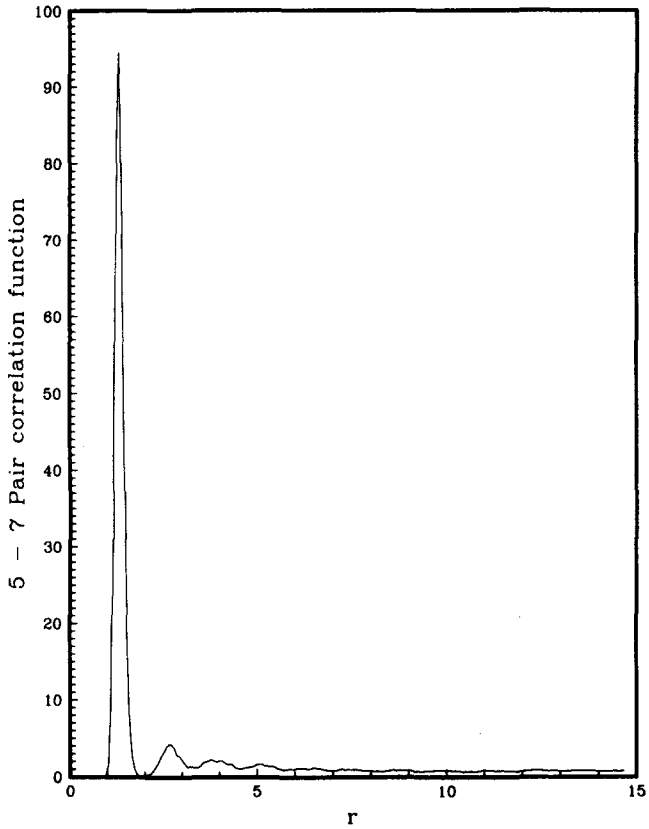

FIG. 10. Pentagon–heptagon pair correlation function g_{57} for the crystalline state A.

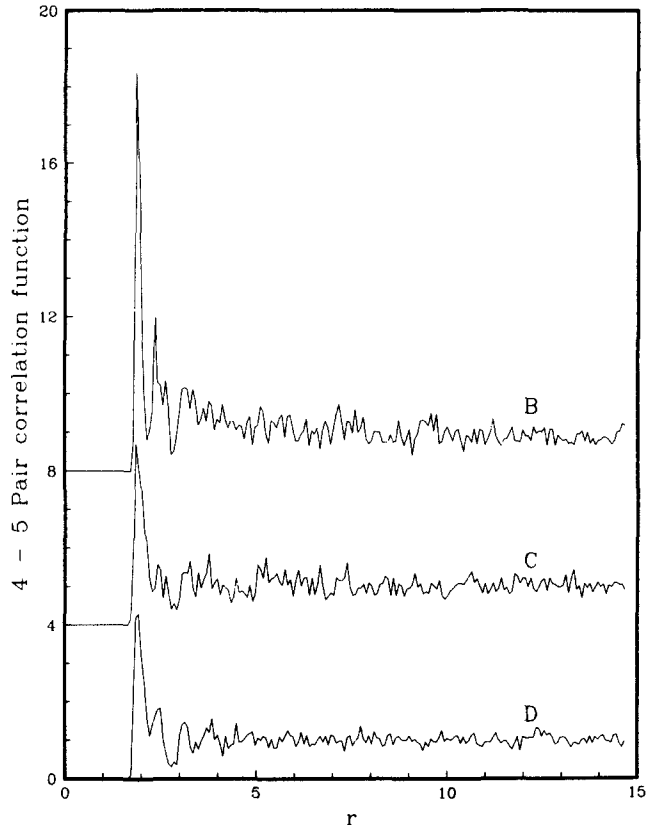

FIG. 12. Quadrilateral–pentagon pair correlation functions g_{45} for states B, C, and D.

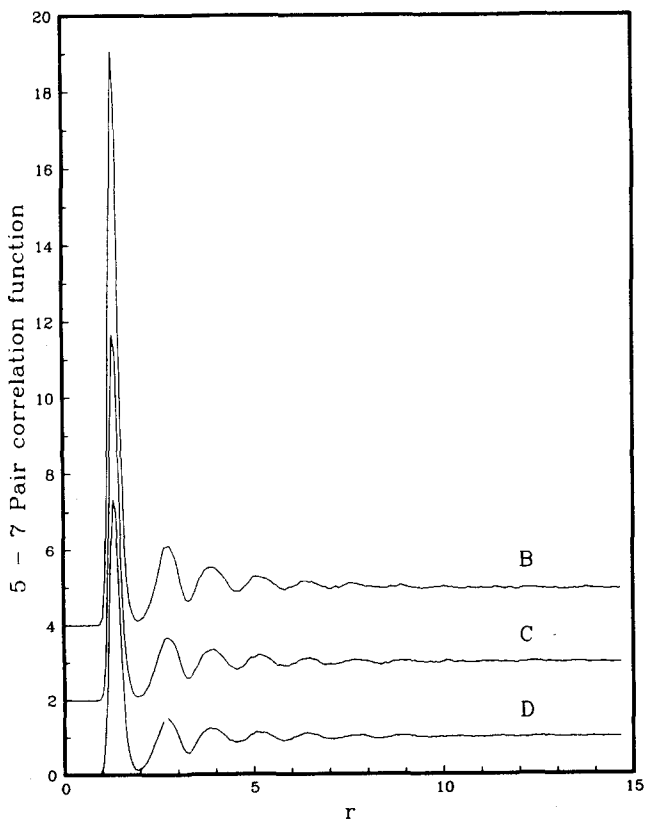

FIG. 11. Pair correlation functions g_{57} for states B, C, and D.

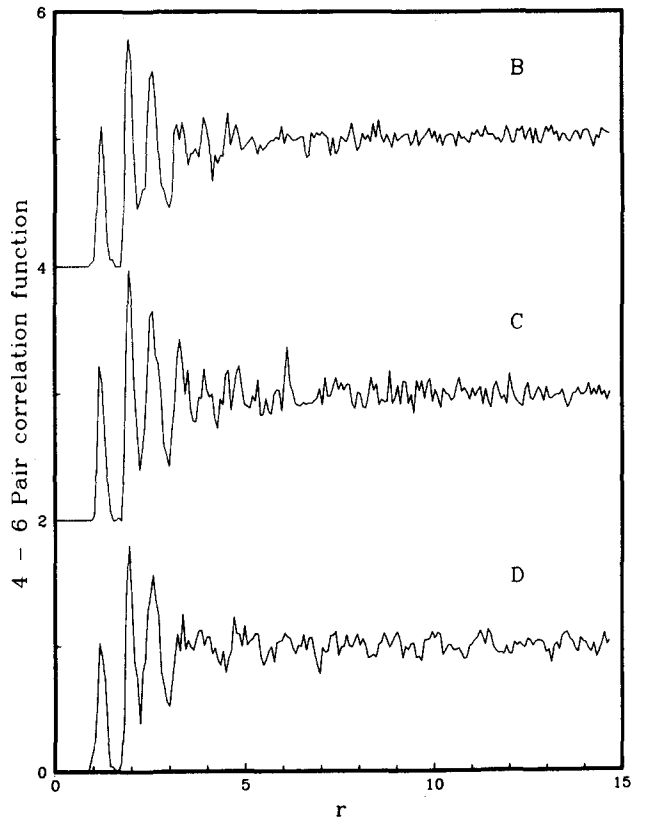

FIG. 13. Quadrilateral–hexagon pair correlation functions g_{46} for states B, C, and D.

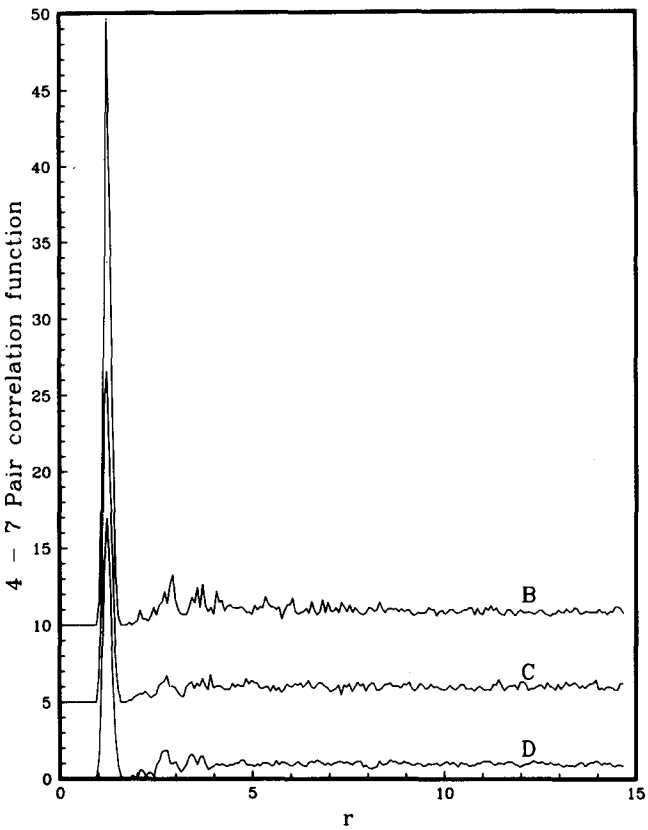

FIG. 14. Quadrilateral–heptagon pair correlations functions g_{47} for states B, C, and D.

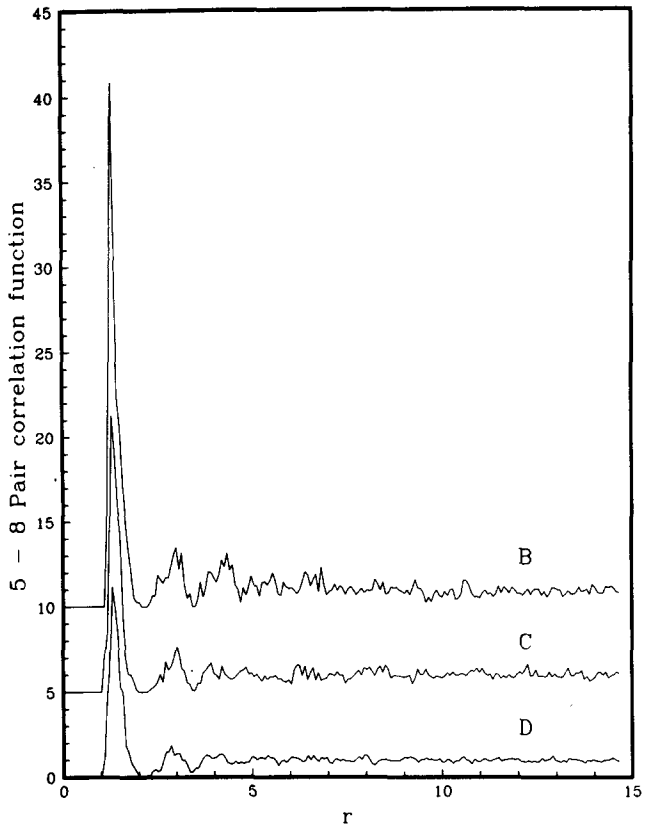

FIG. 15. Pentagon–octagon pair correlation functions g_{58} for states B, C, and D.

to one another; they repel even more strongly than a pair of pentagons. This is revealed by the total absence of *any* peak at roughly the nearest-neighbor distance (c.f., g_{66}). In contrast g_{46} does indeed exhibit a maximum at about the mean nearest-neighbor separation, Fig. 13, though shifted to smaller r as was the case with g_{56}. The g_{47} curves in Fig. 14 show a very strong binding tendency for quadrilaterals and heptagons as nearest neighbors, stronger even than that for 5–7 pairs evident in Fig. 11.

Pair distribution functions involving octagons are presented in Figs. 15–17. Once again no curves are reported for the crystalline state A; in fact *no* octagons appeared during its molecular dynamics run. The expected strong binding of 5–8 pairs shows up clearly in the g_{58} results in Fig. 15. Comparison of g_{58}, g_{68}, and g_{78} in Figs. 15, 16, and 17, respectively, with g_{47}, g_{46}, and g_{45} in Figs. 14, 13, and 12 once again demonstrate breaking of symmetry about $i=6$.

IV. DISCUSSION

The topological condition Eq. (2.1) that the average number of polygon sides is always six may be rewritten in a suggestive manner. For any given polygon α (possessing i_α sides) define

$$\eta_\alpha = i_\alpha - 6 \ . \tag{4.1}$$

Then to within terms of negligible order we must have:

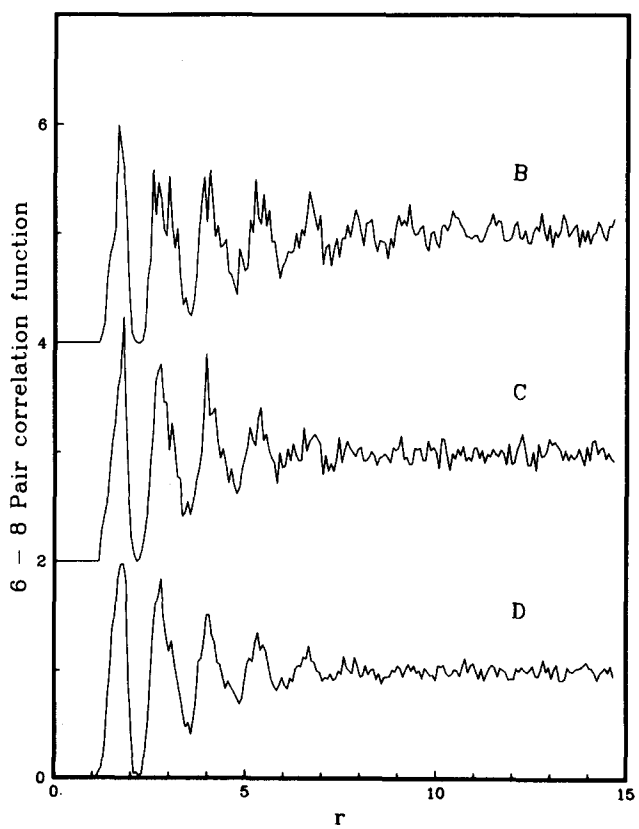

FIG. 16. Hexagon–octagon pair correlation functions g_{68} for states B, C, and D.

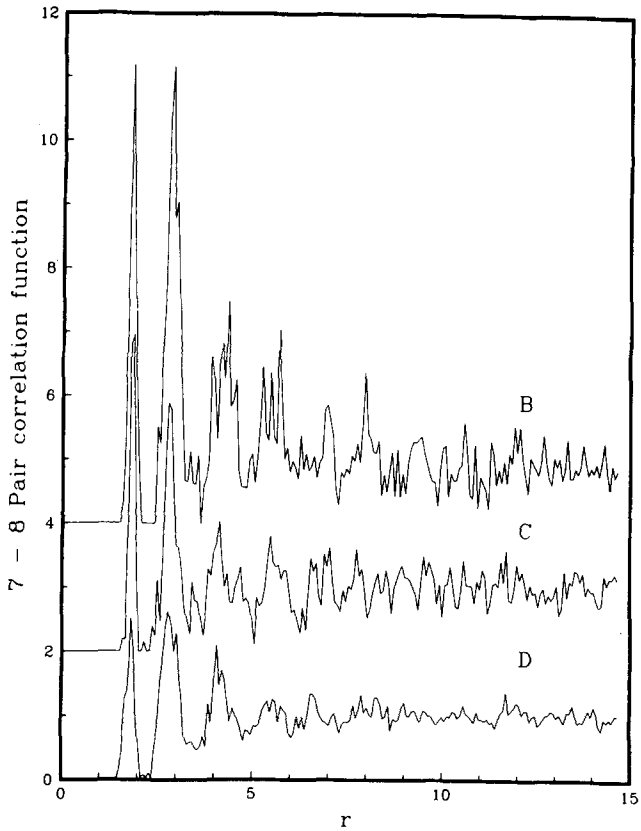

FIG. 17. Heptagon–octagon pair correlation functions g_{78} for states B, C, and D.

$$\sum_{\alpha} \eta_{\alpha} = 0 \,, \tag{4.2}$$

where the sum spans all particles (i.e., polygons) in the system. This is analogous to the charge neutrality condition that applies to electrolytes, with the parameters η_{α} playing the role of electrostatic charges. In this way of reckoning, the topologically perfect crystal acts as pure "solvent" with all particles "uncharged," while disclinations ($i_{\alpha} \neq 6$) are viewed as "ions."

It is the long-range nature of the Coulombic potential between charges that produces an electroneutrality condition in electrolytes and plasmas. Similarly, the existence of condition (4.2) leads one to inquire about long-range interactions between disclinations. Continuum elasticity theory for an isotropic medium in two dimensions leads to the following form for the interaction of two dislocations (Burgers vectors $\mathbf{b}_1$ and $\mathbf{b}_2$)[5,9]:

$$-C_1 \mathbf{b}_1 \cdot \mathbf{b}_2 \ln(r_{12}/a) - C_2 \mathbf{b}_1 \cdot \mathbf{r}_{12}\, \mathbf{r}_{12} \cdot \mathbf{b}_2 / r_{12}^2 \,, \tag{4.3}$$

where C_1, C_2, and a are suitable constants. As noted above, a simple dislocation can be formed from a neighboring 5–7 pair. In order to have expression (4.3) emerge as the interaction of two such 5–7 dyads it is natural to invoke an isotropic disclination–disclination interaction χ that behaves at large distance as

$$\chi(r_{ij}) \sim -K \eta_i \eta_j r_{ij}^2 \ln(r_{ij}/l) \,, \tag{4.4}$$

where K and l are positive. This becomes the appropriate analog of the Coulomb interaction. It is divergent so strongly at large r_{ij} that pairs of opposite disclinations in an otherwise perfect lattice can never unbind, and the same is even true for a dislocation pair if it is to remain in the system at all. In the presence of such long-ranged interactions it would be expected that topological distribution functions would have to obey conditions similar to the exact local electroneutrality and second moment conditions that have been formulated for electrolytes.[10]

The rough similarity between disclinations and ions emboldens one to suggest that the melting of the two-dimensional solid is analogous to the condensation of a dilute salt vapor into a dense molten salt.[11] Both apparently are first order. The electrically neutral diatomic salt molecules and their clusters seen in salt vapors are mirrored in the two-dimensional crystal by a sparse "gas" of 5–7–5–7 tetrads (bound dislocation pairs). Upon condensation of the diatomic salt vapor into the melt the individuality of separate molecules is lost. By the same token individual disolocations are virtually impossible to identify unambiguously in the dense disclination medium that characterizes the two-dimensional fluid.

It remains to be seen if special conditions for two-dimensional melting (specifically the choice of potential) can ever be found to yield a higher order transition analogous to that experienced in the compression of a salt vapor at or above its critical point.

ACKNOWLEDGMENT

We thank Professor John P. McTague for pointing out the utility of Wigner–Seitz polygons in study of the melting transition, and for discussing some of his unpublished results on their distribution patterns.

[1] F. H. Stillinger and T. A. Weber, J. Chem. Phys. 74, 4015 (1981) (preceding paper).
[2] E. Wigner and F. Seitz, Phys. Rev. 43, 804 (1933).
[3] C. Kittel, *Introduction to Solid State Physics*, 2nd ed. (Wiley, New York, 1956), Chap. 19.
[4] B. I. Halperin and D. R. Nelson, Phys. Rev. Lett. 41, 121 (1978); 41, 519 (1978).
[5] D. R. Nelson and B. I. Halperin, Phys. Rev. B 19, 2457 (1979).
[6] J. M. Kosterlitz and D. J. Thouless, J. Phys. C 6, 1181 (1973).
[7] R. Collins, "Melting and Statistical Geometry of Simple Liquids," in *Phase Transitions and Critical Phenomena*, edited by C. Domb and M. S. Green (Academic, New York, 1972), Vol. 2, pp. 271–303.
[8] H. S. M. Coxeter, *Regular Polytopes* (Macmillan, New York, 1963), p. 9.
[9] F. R. N. Nabarro, *Theory of Dislocations* (Clarendon, Oxford, 1967).
[10] F. H. Stillinger and R. Lovett, J. Chem. Phys. 49, 1991 (1968).
[11] *Molten Salt Chemistry*, edited by Milton Blander (Wiley-Interscience, New York, 1964).